Induced superconductivity in Fermi arcs

Z. Faraei[1,*] and S. A. Jafari[1,2,†]

[1]*Department of Physics, Sharif University of Technology, Tehran 11155-9161, Iran*

[2]*Center of Excellence for Complex Systems and Condensed Matter (CSCM), Sharif University of Technology, Tehran 1458889694, Iran*

(Received 19 February 2019; published 31 July 2019)

When the interface of a superconductor (SC) with a Weyl semimetal (WSM) supports Fermi arcs, the chirality blockade eliminates the induction of superconductivity into the bulk of time-reversal symmetry (TRS) breaking WSM. This leaves the Fermi arc states as the only low-energy degrees of freedom in the proximity problem. Therefore the SC|WSM system will be a platform to probe transport properties which involve *only* the Fermi arcs. With a boundary condition that flips the spin at the boundary, we find a Z_2 protected Bogoliubov Fermi contour (BFC) around which the Bogoliubov quasiparticles disperse linearly. The resulting BFC and excitations around it leave a distinct T^2 temperature dependence in their contribution to specific heat. Furthermore, the topologically protected BFC being a Majorana Fermi surface gives rise to a zero-bias peak, the strength of which characteristically depends on the length of Fermi arc and tunneling strength. For the other BC that flips the chirality at the interface, instead of BFCs, we have Bogoliubov-Weyl nodes whose location depends on the tunneling strength.

DOI: 10.1103/PhysRevB.100.035447

I. INTRODUCTION

One of the interesting features of gapless three-dimensional WSMs [1–5] with topologically protected band touching points [6–10] is the realization of robust Fermi arcs [3,11–13]. Angle-resolved photoemission spectroscopy (ARPES) is an appropriate method to observe the Fermi arc shapes [13–15], but for situations where the boundary is buried in the interfaces and, hence, not accessible to ARPES, it is desirable to find the clues of these Fermi arcs in transport experiments. However, the challenge is that when it comes to transport properties, the Weyl cones in the bulk and Fermi arc states both being gapless will jointly contribute to the transport, and therefore, separation of the contribution of surface degrees of freedom is difficult. One of the methods for separating the arc contribution is to address the superconducting proximity effect. In the proximity effect, only several atomic layers near the interface of materials are involved. Therefore, bringing a SC to form a SC|WSM junction, even at this simple-minded level of argument, one expects to observe the Fermi arc dominated effects. As we will argue in this paper, there is yet another more fundamental reason that makes SC|WSM a genuine Fermi arc dominated system for transport purposes.

In recent years, there have been many studies in the issue of superconducting proximity in WSMs, most of which have been focused on the proximity effect on the bulk states. It has been shown that, as long as the conical dispersion (in the bulk excitation spectrum of TRS-broken WSMs) is concerned [16], the Andreev reflection from a conventional *s*-wave superconductors will be blocked: Bovenzi *et al.* [17] have shown that in the proximity with conventional *s*-wave superconductors, if the (momentum) vector connecting the Weyl nodes has a component parallel to the interface (i.e., the interface supports Fermi arcs) the Andreev reflection of bulk degrees of freedom in a TRS-breaking WSM will be suppressed by the phenomenon of *chirality blockade*. The simple explanation of chirality blockade rests on the bulk Hamiltonian of the $\chi\vec{\sigma}\cdot\vec{p}$ form. In proximity to a spin-singlet superconductor, the Andreev reflected hole is required to reverse both spin and physical momentum. The physical momentum reversal is accompanied by chirality flip. But simultaneous reversal of χ, $\vec{\sigma}$, and $\vec{p}$ is not consistent with the conservation of the energy $\chi\vec{\sigma}\cdot\vec{p}$. This will block Andreev reflections involving both momentum *and* spin reversal [17]. However, if the superconductor is not a spin singlet [18], or the Cooper pairs do not have zero center-of-mass momentum (i.e., Fulde-Ferrell-Larkin-Ovchinnikov superconductivity) [19], the chirality blockade will not hold. Other possible ways to escape the chirality blockade would involve pseudoscalar superconductivity [20,21] or Josephson setup [22–24]. Another important situation that spoils the chirality blockade is the presence of a boundary itself [25]. This is simply because the presence of boundary breaks the inversion symmetry.

When the vector connecting the two Weyl nodes is perpendicular to the interface, there would be no chirality blockade [17]. In this situation, there would be no Fermi arcs as well. But once the vector connecting the Weyl nodes develops a small component along the interface (the projection of which is precisely the Fermi arc), the chirality blockade appears. The conclusion will be that the chiraltiy blockade of bulk degrees of freedom in proximity with conventional superconductors crucially depends on the existence of Fermi arcs. So even if the superconducting coherence length is long enough to reach the deep interior of the proximitized system, by chirality blockade in WSMs, the Fermi arc wins the competition,

*zahra.faraei@gmail.com

†akbar.jafari@gmail.com

and the bulk states will have no contributions in induced superconductivity. In this way, the response of a WSM to the proximity with a conventional *s*-wave superconductor *selectively couples to the Fermi arcs only*. From this point of view, the proximity with conventional superconductors can be regarded as a tool to study the transport properties where the only relevant low-energy degrees of freedom are the Fermi arc states. So our proposal in this paper is to promote the SC|WSM heterostructure into a platform to study the transport properties of Fermi arcs only. Motivated by this, we undertake the study of induced superconductivity in the SC|WSM system and find more interesting results than we expected, namely, a topologically protected Bogoliubov Fermi contour (BFC) or Bogoliubov-Weyl (BW) nodes.

Let us start by reviewing the existing literature on the combination of superconductivity with a WSM. The first class of works start by a Weyl system which are superconducting in the *bulk* and examine the resulting surface states [18,26,27]. In this class of works, doping a WSM converts the flatband along the nodal direction to crossing flatbands [28]. This can be understood in terms of the nontrivial monopole charge of the Cooper pairs [29]. In this paper, we are not concerned with this class.

The second class, however, deals with the induction of superconductivity in WSMs and their surface states (Fermi arc states). The numerical result of Khanna and co-workers indicates that the Fermi arc states are gapped except for the two points corresponding to the projection of Weyl nodes on the surface supporting the Fermi arcs [23]. The presence of gapless points in the excitations of the Bogoliubov quasiparticle spectrum of a WSM can be understood as follows: A generic gap term in the Dirac equation has to be proportional to $\psi_R^*\psi_L$ [30] which corresponds to a term, such as $\psi_R^*\psi_R^*$. This is because the complex conjugation exchanges the chirality [30]. But these types of terms are forbidden if one requires zero center-of-mass Cooper pairs [31]. Therefore, the spectrum of Bogoliubov excitations in the WSM cannot be entirely gapped, and there should exist nodal points or nodal lines.

In this paper, we will develop an analytical understanding of the induced superconductivity in Fermi arc states of undoped WSMs. The analytical approach of the present paper based on classification of boundary conditions (BCs) in WSMs [32–34] and their Greens' function [32] will enable us—depending on the BC—to obtain elliptic BFC or BW nodes. We find that, for first-type BC that flips the spin at the boundary, the BFC is protected by a Z_2 index and find an appropriate Pfaffian that changes sign across the BFC. For this type of BC, the Bogoliubov excitations around the BFC are linearly dispersing and, therefore, contribute a specific-heat term that can be distinguished from bulk contributions. For the second-type of BC that flips the chirality at the boundary, instead of robust BFC, we find pairs of BW nodes that disperse by changing the tunneling strength. For mixed BC, there will be a phase transition that separates the above two situations.

The paper is organized as follows: In Sec. II, we adjust our previously developed Green's function method for problems involving the superconductivity. In Sec. III, we bring the SC into proximity with the WSM, and, corresponding to two classes of BCs, we obtain the nature of superconductivity induced into Fermi arc states. In Sec. IV, we talk about pairing symmetry and discuss the Majorana character of the BFC. We end the paper with a summary of the main findings in Sec. V. Details of algebra are presented in the Appendix.

II. GREEN'S FUNCTION METHOD

A. Green's function for electrons

In our previous work [32], we have calculated the Green's function of a normal WSM. Since the present paper will be based on our earlier work, let us briefly summarize its core results. For a semi-infinite inversion symmetric WSM with two nodes at $\pm\vec{b}$ and a hard wall boundary [33] at $z = 0$, the wave equation is as follows:

$$[i\hat{\tau}_z \otimes (\vec{\sigma}\cdot\vec{\nabla}) + \hat{\tau}_0 \otimes (\vec{\sigma}\cdot\vec{b}) + \check{M}\delta(z)]\psi_e = E\psi_e, \tag{1}$$

where $\check{M}$ is a 4×4 Hermitian unitary matrix and effectively incorporates the confinement potential at the boundary. Pauli matrices τ and σ operate in chirality and spin spaces. We work in units of $\hbar = 1$. Furthermore, the lengths and velocities are measured in units of $|\vec{b}|^{-1}$ and v_F, respectively. The electron wave-function ψ_e is a four-component wave function,

$$\psi_e = [\psi_{-\uparrow}, \psi_{-\downarrow}, \psi_{+\uparrow}, \psi_{+\downarrow}]^T,$$

where $\pm$'s represent the chirality corresponding to right-handed and left-handed fermions and $\uparrow, \downarrow$ denote the spin direction.

Consistency with the constraint of hard wall assumption, gives the following form for the boundary matrix $\check{M}$ [20]:

$$\check{M} = (\cos\gamma)\check{M}_1 + (\sin\gamma)\check{M}_2, \tag{2}$$

where

$$\check{M}_1 = \begin{pmatrix} 0 & e^{-i\Lambda} & 0 & 0 \\ e^{i\Lambda} & 0 & 0 & 0 \\ 0 & 0 & 0 & e^{-i\xi} \\ 0 & 0 & e^{i\xi} & 0 \end{pmatrix} \tag{3}$$

rotates the in-plane component of the spin through angles $\Lambda = -\cot^{-1}(b_y/b_x)$ and $\xi = \Lambda - \pi$ for the left- and right-handed electrons, respectively, and

$$\check{M}_2 = \begin{pmatrix} 0 & 0 & e^{-i\alpha} & 0 \\ 0 & 0 & 0 & e^{-i\beta} \\ e^{i\alpha} & 0 & 0 & 0 \\ 0 & e^{i\beta} & 0 & 0 \end{pmatrix}, \tag{4}$$

which is diagonal in spin space, but mixes the chirality components. Independent of the value of γ, the BC Eq. (2) frightfully reproduces a Fermi arc on the surface state that connects the projections of Weyl nodes on the surface [32]. Requiring the Fermi arc (ray) emitted from one node to end precisely at the other node gives $\alpha - \beta = \Lambda - \xi$.

For the Hamiltonian Eq. (1), the time-ordered single-particle Green's function of electrons is given by

$$\hat{G}^{\sigma\sigma'}_{\chi\chi'}(\vec{r},\vec{r}\,') = G^{\sigma\sigma'}_{\chi\chi'}(z,z')e^{[ik_x(x-x')+ik_y(y-y')]}, \tag{5}$$

where

$$G^{\bar{\sigma}\sigma}_{\chi\chi'}(z,z') = C^{\bar{\sigma}\sigma}_{\chi\chi'}(z')e^{-(q_\chi+i\chi b_z)z} - \frac{\chi\left(k_x^\chi + i\sigma k_y^\chi\right)}{8\pi^2(q_\chi+i\chi b_z)}e^{-(q_\chi+i\chi b_z)|z-z'|}\delta_{\chi\chi'}, \tag{6}$$

and

$$G^{\sigma\sigma}_{\chi\chi'}(z,z') = \frac{\varepsilon - i\chi\sigma\partial_z + \sigma b_z}{\chi\left(k_x^\chi + i\sigma k_y^\chi\right)} G^{\bar\sigma\sigma}_{\chi\chi'}(z,z'), \tag{7}$$

where $\chi, \chi' = \pm 1$ is the chirality, $\sigma = \pm 1$ represents the spin direction, $\bar\sigma = -\sigma$, and $q_\chi = (k_x - \chi b_x)^2 + (k_y - \chi b_y)^2 - \epsilon^2$. ϵ is the electron's energy. Since we consider a system that is infinite in the x and y directions, the momenta along the x and y axes are good quantum numbers, and a plane-wave part can be factorized in Eq. (5).

The coefficients $C^{\sigma\sigma'}_{\chi\chi'}$ depend on the BC. For $\check M_1$-type BC ($\gamma = 0$), we have

$$C^{\bar\sigma\sigma}_{\chi\chi'} = \frac{\varepsilon - i\chi\sigma q_\chi + 2\sigma b_z - \chi e^{-i\sigma\theta_\chi}\left(k_x^\chi + i\sigma k_y^\chi\right)}{\varepsilon + i\chi\sigma q_\chi - \chi e^{-i\sigma\theta_\chi}\left(k_x^\chi + i\sigma k_y^\chi\right)} \times \frac{\chi\left(k_x^\chi + i\sigma k_y^\chi\right)}{8\pi^2(q_\chi + i\chi b_z)} e^{-(q_\chi + i\chi b_z)z'}\delta_{\chi\chi'}, \tag{8}$$

whereas, for $\check M_2$-type BC ($\gamma = \pi/2$), one obtains

$$C^{\bar\sigma\sigma}_{\chi\chi} = \frac{i\chi\sigma\left(k_x^\chi + i\sigma k_y^\chi\right)\left(k_x^{\bar\chi} + i\sigma k_y^{\bar\chi}\right)}{8\pi^2 D^{\bar\sigma\sigma}_{\chi\chi}} e^{-(q_\chi + i\chi b_z)z'}, \tag{9}$$

$$C^{\bar\sigma\sigma}_{\bar\chi\chi} = \frac{\chi\left(k_x^\chi + i\sigma k_y^\chi\right)}{8\pi^2(q_\chi + i\chi b_z)}\left(\frac{N^{\bar\sigma\sigma}_{\chi\chi}}{D^{\bar\sigma\sigma}_{\chi\chi}}\right) e^{-(q_\chi + i\chi b_z)z'}, \tag{10}$$

where

$$D^{\bar\sigma\sigma}_{\chi\chi} = \bar\chi e^{i\chi\theta_{\bar\sigma}}(\varepsilon + i\chi\sigma q_\chi)\left(k_x^{\bar\chi} + i\sigma k_y^{\bar\chi}\right) - \chi e^{i\chi\theta_\sigma}(\varepsilon + i\bar\chi\sigma q_{\bar\chi})\left(k_x^\chi + i\sigma k_y^\chi\right), \tag{11}$$

and

$$N^{\bar\sigma\sigma}_{\chi\chi} = D^{\bar\sigma\sigma}_{\chi\chi} + 2i\sigma e^{i\chi\theta_{\bar\sigma}}(q_\chi + i\chi b_z)\left(k_x^{\bar\chi} + i\sigma k_y^{\bar\chi}\right). \tag{12}$$

Both BCs produce a Fermi ray (meaning that the shape of the Fermi arc is a straight line) connecting the projection of Weyl nodes on the surface whose slope is solely determined by vector $\vec b$ as $\tan^{-1}(b_y/b_x)$.

B. Green's functions for holes

To incorporate superconductivity into our Green's function formulation, we need to augment the Green's functions into the Nambu space. So, we need the Green's function for the holes as well. The electron and hole Hamiltonians are related by the operation of time-reversal operator [17],

$$H_h(\vec k) = \sigma_y H_e^*(-\vec k)\sigma_y. \tag{13}$$

For the Weyl Hamiltonian in Eq. (1), the corresponding hole Hamiltonian becomes

$$H_h(\vec k) = \tau_z(\vec\sigma\cdot\vec k) - \tau_0(\vec\sigma\cdot\vec b), \tag{14}$$

which can be combined with the electronic part to give the Bogoliubov–de Gennes (BdG) Hamiltonian,

$$H_W = \begin{pmatrix} H_e & 0 \\ 0 & -H_h \end{pmatrix}. \tag{15}$$

The crucial point in constructing the Green's function for holes is that the particle-hole transformation should also operate on matrix $\check M$ in Eq. (1) that encodes the BC information. Starting with BC matrix $\check M_1$ of electrons,

$$\check M_1 = \frac{\hat\tau_0 + \hat\tau_z}{2} \otimes (\cos\Lambda\hat\sigma_x + \sin\Lambda\hat\sigma_y) + \frac{\hat\tau_0 - \hat\tau_z}{2} \otimes (\cos\xi\hat\sigma_x + \sin\xi\hat\sigma_y)$$

for holes we obtain $\sigma_y\check M_1^*\sigma_y = -\check M_1$ which is eventually equivalent to the substitutions $\Lambda \to \pi + \Lambda$ and $\xi \to \pi + \xi$. This is quite intuitive as the reflection of an electron with its in-plane spin rotated by angle Λ after the TR operation can be equivalently viewed as rotation of the spin of a hole by angle $\pi + \Lambda$. Similarly, for $\check M_2$-type BC, we have

$$\check M_2 = (\cos\alpha\hat\tau_x + \sin\alpha\hat\tau_y) \otimes \frac{\hat\sigma_0 + \hat\sigma_z}{2} + (\cos\beta\hat\tau_x + \sin\beta\hat\tau_y) \otimes \frac{\hat\sigma_0 - \hat\sigma_z}{2}$$

which upon particle-hole transformation becomes

$$\sigma_y\check M_2^*\sigma_y = (\cos\alpha\hat\tau_x - \sin\alpha\hat\tau_y) \otimes \frac{\hat\sigma_0 - \hat\sigma_z}{2} + (\cos\beta\hat\tau_x - \sin\beta\hat\tau_y) \otimes \frac{\hat\sigma_0 + \hat\sigma_z}{2}.$$

Therefore, the $\check M_2$ BC matrix for holes is obtained from the corresponding $\check M_2$ of electrons by the replacement $\alpha \leftrightarrow -\beta$.

Now, we are ready to set up the Green's function for holes. For this, we need to solve

$$[\varepsilon + H_h + \check M_h\delta(z)]G_h = \delta(\vec r - \vec r'),$$

where the matrix $\check M_h$ can be any of the matrices discussed above. Another important technical point is that the hole part of the wave function is as follows:

$$\psi_h = [-\psi^*_{+\downarrow}, \psi^*_{+\uparrow}, -\psi^*_{-\downarrow}, \psi^*_{-\uparrow}]^T.$$

So that $\check G_h(\vec r, \vec r\,')$ will be arranged into the following matrix:

$$\check G_h(\vec r, \vec r\,') = \begin{pmatrix} [\hat G_{++}(\vec r, \vec r\,')]_h & [\hat G_{+-}(\vec r, \vec r\,')]_h \\ [\hat G_{-+}(\vec r, \vec r\,')]_h & [\hat G_{--}(\vec r, \vec r\,')]_h \end{pmatrix}. \tag{16}$$

In the above equation, $[\hat G_{\chi\chi'}(\vec r, \vec r\,')]_h$ is of the following form:

$$[\hat G_{\chi\chi'}]_h = \begin{pmatrix} G^{\downarrow\downarrow}_{\chi\chi'}(z,z') & G^{\downarrow\uparrow}_{\chi\chi'}(z,z') \\ G^{\uparrow\downarrow}_{\chi\chi'}(z,z') & G^{\uparrow\uparrow}_{\chi\chi'}(z,z') \end{pmatrix} e^{[ik_x(x-x') + ik_y(y-y')]}, \tag{17}$$

where every element in the above equation is obtained from the corresponding element of the electron Green's function by appropriate replacements of the angles as discussed above. After this replacement (and, of course, changing the sign of energy), the spin-off-diagonal elements of the holes Green's functions become

$$G^{\bar\sigma\sigma}_{\chi\chi'}(z,z') = C^{\bar\sigma\sigma}_{\chi\chi'}(z')e^{-(q_\chi + i\chi b_z)z} - \frac{\chi\left(k_x^\chi - i\sigma k_y^\chi\right)}{8\pi^2(q_\chi + i\chi b_z)} e^{-(q_\chi + i\chi b_z)|z - z'|}\delta_{\chi\chi'}, \tag{18}$$

whereas the spin-diagonal components are as follows:

$$G^{\sigma\sigma}_{\chi\chi'}(z,z') = \frac{\varepsilon + i\chi\sigma\partial_z - \sigma b_z}{\chi\left(k_x^\chi - i\sigma k_y^\chi\right)} G^{\bar\sigma\sigma}_{\chi\chi'}(z,z'), \tag{19}$$

where $k^{\chi}_{x(y)} = k_{x(y)} + \chi b_{x(y)}$. The value of these matrix elements is the same as those for electrons, except for the replacement $\sigma \to -\sigma$.

Up to this point, the above expressions are valid for any BC. For $\check{M}_1$-type BC, we have

$$C^{\bar{\sigma}\sigma}_{\chi\chi'} = \frac{\varepsilon + i\chi\sigma q_\chi - 2\sigma b_z - \chi e^{i\sigma\theta_\chi}\left(k^\chi_x - i\sigma k^\chi_y\right)}{\varepsilon - i\chi\sigma q_\chi - \chi e^{i\sigma\theta_\chi}\left(k^\chi_x - i\sigma k^\chi_y\right)} \times \frac{\chi\left(k^\chi_x - i\sigma k^\chi_y\right)}{8\pi^2(q_\chi + i\chi b_z)} e^{-(q_\chi + i\chi b_z)z'}\delta_{\chi\chi'}, \tag{20}$$

where $\theta_- = \Lambda + \pi$ and $\theta_+ = \xi + \pi$ and for the $\check{M}_2$-type BC for chirality off-diagonal and chirality off-diagonal, respectively, we obtain

$$C^{\bar{\sigma}\sigma}_{\bar{\chi}\chi} = \frac{-i\chi\sigma\left(k^\chi_x - i\sigma k^\chi_y\right)\left(k^{\bar{\chi}}_x - i\sigma k^{\bar{\chi}}_y\right)}{8\pi^2 D^{\bar{\sigma}\sigma}_{\chi\chi}} e^{-(q_\chi + i\chi b_z)z'}, \tag{21}$$

$$C^{\bar{\sigma}\sigma}_{\chi\chi} = \frac{\chi\left(k^\chi_x - i\sigma k^\chi_y\right)}{8\pi^2(q_\chi + i\chi b_z)}\left(\frac{N^{\bar{\sigma}\sigma}_{\chi\chi}}{D^{\bar{\sigma}\sigma}_{\chi\chi}}\right) e^{-(q_\chi + i\chi b_z)z'}, \tag{22}$$

where

$$D^{\bar{\sigma}\sigma}_{\chi\chi} = \bar{\chi} e^{i\chi\theta_{\bar{\sigma}}}(\varepsilon - i\chi\sigma q_\chi)\left(k^{\bar{\chi}}_x - i\sigma k^{\bar{\chi}}_y\right) - \chi e^{i\chi\theta_\sigma}(\varepsilon - i\bar{\chi}\sigma q_{\bar{\chi}})\left(k^\chi_x - i\sigma k^\chi_y\right), \tag{23}$$

and

$$N^{\bar{\sigma}\sigma}_{\chi\chi} = D^{\bar{\sigma}\sigma}_{\chi\chi} - 2i\sigma e^{i\chi\theta_{\bar{\sigma}}}(q_\chi + i\chi b_z)\left(k^{\bar{\chi}}_x - i\sigma k^{\bar{\chi}}_y\right), \tag{24}$$

with $\theta_\uparrow = -\beta$ and $\theta_\downarrow = -\alpha$.

For practical calculations, one has to specialize to a specific coordinate system. The coordinate system can be chosen in such a way that the Fermi arc lies along the k_x axis. This does not harm the generality of approach as always by appropriate rotation along the k_z axis, a new coordinate system can be chosen in such a way that the new k_x is along the Fermi arc. For details, please refer to the Appendix.

III. PROXIMITY WITH A SUPERCONDUCTOR

Now, we bring a conventional s-wave SC near the WSM. The SC occupies the $z > 0$ part of the space, and WSM occupies the $z < 0$ part with its interface being at $z = 0$. The bulk Hamiltonian of the SC is as follows:

$$H_s = [|\vec{k}_s|^2/(2m)\hat{\kappa}_3 + \Delta_s\hat{\kappa}_1] \otimes \hat{\sigma}_0, \tag{25}$$

where $\vec{k}_s$ denotes the momentum in the SC, m is the electron mass, Δ_s is the superconducting gap, and $\hat{\kappa}_{(i=0\cdots3)}$ are the Pauli matrices acting in the particle-hole space. The coupling between WSM and SC is incorporated by

$$\mathcal{T} = \begin{pmatrix} 0 & \check{t}^\dagger \\ \check{t} & 0 \end{pmatrix}, \tag{26}$$

where, considering that the tunneling amplitude t is the same for right-handed and left-handed electrons, the 4×8 matrix $\check{t}$ is constructed as $\check{t} = t/2(\check{t}_+ \; \check{t}_-)$ from 4×4 matrices $\check{t}_\alpha = (\hat{\tau}_z + \alpha\hat{\tau}_0 + \hat{\tau}_1 + i\alpha\hat{\tau}_y) \otimes \hat{\sigma}_0$ with $\alpha = \pm$.

Based on the Dyson equation, the Green's function of the WSM becomes

$$\mathcal{G}_W = \mathcal{G}^0_W + \sum_{k_s} \mathcal{G}^0_W \check{t}^\dagger \check{g}_s \check{t} \mathcal{G}_W, \tag{27}$$

where we use the symbols $\check{g}_s$ to denote 4×4 matrices and $\mathcal{G}$ for 8×8 matrices. The superscript 0 in $\mathcal{G}^0$ denotes the Green's function in Nambu space when the tunneling is set to zero.

Assuming that the superconductivity at the surface of the SC is of the same form as its bulk and that $\check{t}$ and $\check{t}^\dagger$ in Eq. (27) are independent of $\vec{k}_s$, we can perform the sum over $\vec{k}_s$ to obtain the self-energy as [35]

$$\sum_{k_s} \check{t}^\dagger \check{g}_s \check{t} = \frac{s}{\sqrt{\Delta^2 - \epsilon^2}}(\epsilon\hat{\kappa}_0 - \Delta\hat{\kappa}_1) \otimes (\hat{\tau}_0 + \hat{\tau}_x) \otimes \hat{\sigma}_0, \tag{28}$$

where $s = \pi\rho_0 t$ with ρ_0 as the density of states of the superconductor at its Fermi level before becoming a superconductor. Substituting this result in Eq. (27), we can drive the Green's function for the surface of the WSM in the presence of a SC.

A. $\check{M}_1$-type BC

The poles of the Green's function give us the dispersion relation of the excitations on the surface. For $\check{M}_1$-type BC, we obtain the following secular equation for the poles of the Green's function:

$$[\mathcal{F}(\epsilon, \vec{k}) + 4\epsilon b k_y s^2]^2 - 16 s^4 \epsilon^4 \left(k_x^2 + k_y^2\right) = 0, \tag{29}$$

where $\mathcal{F}(\epsilon, \vec{k}) = \sqrt{\Delta^2 - \epsilon^2}[4s^4(-b^2 + k_x^2 + k_y^2) - (\epsilon^2 - k_y^2)]$ and the tunneling strength s quantifies the ability of electrons in the superconductor to tunnel into the WSM. The states at the Fermi level correspond to $\epsilon = 0$, such that the above equation becomes $\mathcal{F}^2(0, \vec{k}) = 0$. Therefore, the solutions of $\mathcal{F}(0, \vec{k}) = 0$ will be twofold degenerate. These solutions are

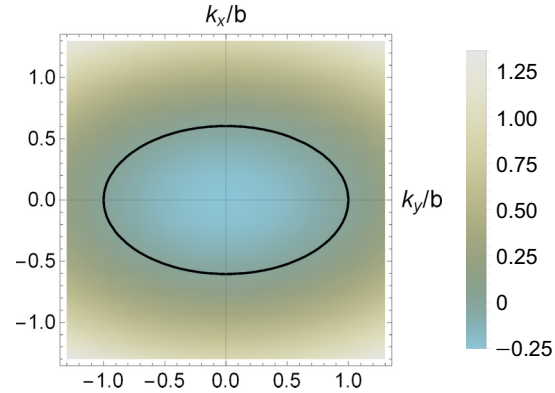

FIG. 1. Bogoliubov Fermi contour for the first-type boundary conditions. The major axis of the ellipse coincides with the Fermi arc of the WSM before bringing the SC to contact with it. The Pfaffian (see the text) changes sign across this contour, and excitations around the elliptic contour are linearly dispersing. The minor axis of the ellipse depends on the tunneling strength as in Eq. (30). By turning off the tunneling, the minor axis becomes zero, and the ellipse will reduce to the Fermi arc.

given by the following ellipse on the k_x-k_y plane (see Fig. 1):

$$k_x^2 + \left(\frac{1+4s^4}{4s^4}\right)k_y^2 = 1. \tag{30}$$

The major axis of this ellipse is horizontal with magnitude 1 (note that, in our units, a momentum of size 1 actually means b) and coincides with the Fermi arc of the pristine Weyl semimetal before bringing the superconductor to its proximity. This is similar to the zero-energy surfaces due to Fermi arcs of the *doped* WSM [29]. Furthermore, the magnitude of the minor axis $\tilde{b} = \frac{2s^2}{\sqrt{1+4s^4}}$ is determined by the combination s of the tunneling amplitude t and the density of states ρ_0 of the superconductor in its normal phase. As such, when the superconducting agent is an undoped Dirac superconductor [20], due to $\rho_0 = 0$, the minor axis will be of zero length, and the ellipse will collapse into the Fermi arc. It is curious that, although the very existence of the ellipse depends on the superconducting gap Δ of the s-wave superconductor that proximitizes the WSM, the minor axis does not depend on the superconducting gap Δ and is only controlled by the tunneling strength s.

At $\epsilon = 0$, the denominator of Green's function $(\epsilon - H)^{-1}$ will become the determinant of the Hamiltonian, i.e., $\mathcal{F}^2(0,\vec{k}) = \det H(\vec{k})$, where $H(\vec{k})$ is the Hamiltonian of the entire system. The above relations mean that $\mathcal{F}(0,\vec{k})$ is actually the Pfaffian of the Hamiltonian. Following Refs. [36,37], we use $\mathcal{F}(0,\vec{k})$ to construct the Z_2 topological index ν that protects the zero-energy ellipse of Bogoliubov quasiparticles as $(-1)^\nu = \mathrm{sgn}[\mathcal{F}(\vec{k}_-)\mathcal{F}(\vec{k}_+)]$ where $\vec{k}_+(\vec{k}_-)$ refers to momenta inside (outside) the BFC [36,37]. As can be seen, $\mathcal{F}(0,\vec{k})$ changes its sign across the elliptic zero-energy contour, and therefore, we are dealing with the $\nu = -1$ situation which is Z_2 nontrivial. In our two-dimensional case, the Z_2 index is only consistent with the DIII class which belongs to the BdG family [38,39]. In this class, particle-hole and sublattice symmetries must be present which is here the case by construction. The TR must be broken, which is here again the case, as the parent WSM is characterized by TR breaking parameter $\vec{b}$. The meaning of $\nu = -1$ is that weak perturbations within the DIII class are not able to destroy the elliptic Fermi contour of Bogoliubov quasiparticles. A simple consequence of this robustness is that by changing the tunneling parameter s, only the minor axis of the ellipse changes, but it cannot be cut into pieces or destroyed. As we will see in next subsection with $\check{M}_2$-type BC, we will have a totally different situation.

In terms of the Altland-Zirnbauer [40] classification, the induced superconductivity on Fermi arc states belongs to the DIII class. The interpretation of its Z_2 index is connected with the existence of (elliptic) BFC. Once the Fermi contour is formed, the Fermi contour *itself* as a singularity of the Green's function in momentum space can be further classified by a winding number [41]. This is defined by

$$n_1 = \mathrm{tr}\frac{1}{2\pi i}\oint_C G\,\partial_\ell G^{-1} d\ell, \tag{31}$$

where the closed path C is any contour enclosing the Fermi contour (ellipse in our case) and ℓ parametrizes this path. For the Fermi contour of two-dimensional metals, as long as it has the Fermi-liquid structure $G(i\omega, p) \propto (i\omega - p)^{-1}$, where p is the momentum deviation from the Fermi contour, the above winding number will be ± 1. However, an essential difference between the elliptic Fermi contour of Bogoliubov quasiparticles compared to the Fermi contour of Fermi liquids is that, due to twofold degeneracy, the pole structure near the Fermi contour is given by $G(i\omega, p) \propto (i\omega - p)^{-2}$. This form of the Fermi contour will give $n_1 = \pm 2$. This means that, in principle, there can be perturbations outside the DIII class which can break the $n_1 = 2$ topological charge into two $n_1 = 1$ (Fermi-liquid-like) Fermi contours.

To gain further insight into the physical nature of this BFC, let us study the excitations around this elliptic Fermi contour. In the radial direction, a little away from the ellipse, we can use a small parameter η to parametrize the momenta at $\epsilon = 0$ as $k_x = (1+\eta)\cos\phi$ and $k_y = (\tilde{b}+\eta)\sin\phi$. Let us assume that, by approaching the ellipse, energy vanishes as $\alpha\eta^\gamma$. With this choice, the lowest-order terms of Eq. (29) are as follows:

$$\begin{aligned}&\frac{4\tilde{b}^4}{1-\tilde{b}^2}\alpha^2\eta^{2\gamma}\sin^2\phi + \left(\frac{2\,\Delta\tilde{b}^2}{1-\tilde{b}^2}\right)^2\eta^2\left(\cos^2\phi + \frac{1}{\tilde{b}}\sin^2\phi\right)^2 \\ &\quad + \left[\frac{8\Delta\tilde{b}^4}{(1-\tilde{b}^2)^{3/2}}\right]\alpha\eta^{\gamma+1}\left(\cos^2\phi + \frac{1}{\tilde{b}}\sin^2\phi\right)\sin\phi \\ &= \frac{4\tilde{b}^2}{1-\tilde{b}^2}\alpha^4\eta^{4\gamma}\left(\cos^2\phi + \frac{1}{\tilde{b}}\sin^2\phi\right).\end{aligned} \tag{32}$$

If $\gamma > 1$, then only the second term on the left-hand side is the leading-order term and should be zero, but it is generically impossible. On the other hand, if $\gamma < 1$, then the first term in Eq. (32) is the leading-order term, and this leads to $\alpha = 0$. We, thus, conclude that $\gamma = 1$ and that around the BFC the energy disperses linearly. There are only two exceptions to $\gamma = 1$: at $\phi = 0$ (and $\phi = \pi$ related to the former by symmetry) which correspond to dispersion along the k_x axis. These two peculiar points correspond to the projection Weyl nodes on the k_x-k_y surface. In this case, $\sin\phi = 0$, and Eq. (32) reduces to

$$\left(\frac{\Delta\tilde{b}^2}{1-\tilde{b}^2}\right)\eta^2 = \alpha^4\eta^{4\gamma}, \tag{33}$$

from which we obtain $\gamma = 1/2$. Therefore, the singular behavior at $\phi = 0$ means that, by departing from the projection of Weyl nodes in the k_x direction inward of the ellipse, we obtain a peculiar $\varepsilon(p_x, p_y = 0) \sim \sqrt{p_x}$ where p_x and p_y measure the momenta from the two ends of the major axis of the ellipse.

B. $\check{M}_2$-type BC

Unlike the $\check{M}_1$-type BC where a robust BFC is obtained which can be distorted but not destroyed by changing the parameters of the Hamiltonian (in our case, the combination $s = \pi\rho_0 t$), for $\check{M}_2$-type BC, instead of BFC, we will have a set of BW nodes. To see this, let us look into the zeros of the determinant appearing in the denominator of the Green's function, which, at $\epsilon = 0$, becomes

$$\begin{aligned}&\left\{\left[3\left(b^2 - k_x^2 + ky^2\right)^2 + 4k_x^2\left(b^2 - 4k_y + 3k_y^2\right)\right]s^4 - b^2k_y^2\right\}^2 \\ &\quad + 16b^2k_x^2k_y^2(2k_y - b)^2s^4 = 0.\end{aligned} \tag{34}$$

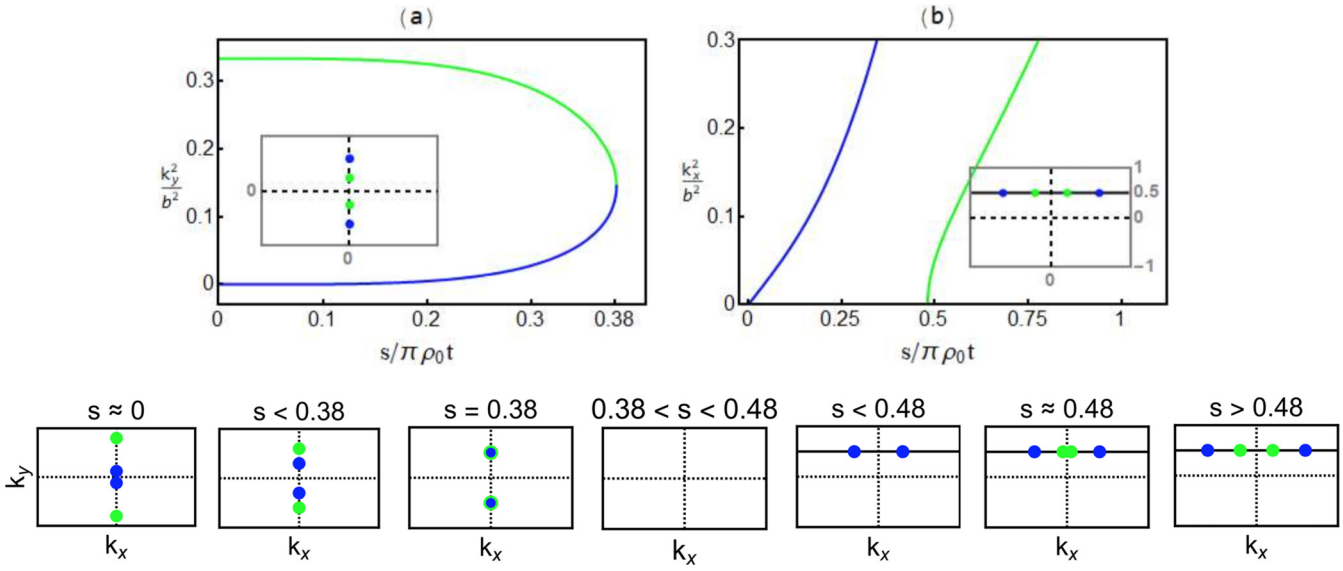

FIG. 2. Bogoliubov-Weyl nodes with second-type boundary conditions. (a) The k_y^2 coordinate of the position of BW nodes as a function of dimensionless tunneling strength s. (b) The k_x^2 coordinate of the nodes lying on $k_y = b/2$ as a function of s. The insets in both (a) and (b) indicate the locations of BW nodes. The panels in the second row show the schematic evolution of BW nodes upon varying s. Colors of the nodes correspond to their chirality.

This expression being the sum of two complete squares appearing in the first and second lines, respectively, can only vanish when each term separately vanishes. From the second line, there are three possibilities, namely, $k_x = 0$, $k_y = b/2$, or $k_y = 0$. The third case does not give any zero for the first line. The first two cases, however, give two pairs of solutions as follows (note that we are working in units of $b = 1$): On the $k_x = 0$ line, there are two values of k_y^2 as long as tunneling is less than $s_{\max} = [(4 - \sqrt{15})/6]^{1/4} \approx 0.38$. As can be seen in Fig. 2(a), the two solutions move towards each other and hit at $s_{\max}$. Beyond $s_{\max}$, there is no zero-energy solution on the k_y axis, meaning that the two BW nodes annihilate each other upon colliding. This indicates that they are carrying opposite topological charges. Their partner on the negative k_y axis also behaves similarly. This has been schematically shown in the second row of Fig. 2. On the $k_y = 1/2$ line, as can be see in Fig. 2(b), the blue pair of BW nodes start at $k_x^2 \approx 0$ for very small $s \approx 0$. As can be seen, k_x^2 increases linearly as we increase s. Beyond $s_{\min} = (4/75)^{1/4} \approx 0.48$, a second pair of (green) BW nodes appear on $k_y = 1/2$ and start their journey from the $k_x^2 = 0$ point. By further increasing s, the blue and green BW nodes further depart from each other.

C. Linear combination of $\check{M}_1$-type and $\check{M}_2$-type BCs

Let us now see what happens if the boundary condition is neither $\check{M}_1$ nor $\check{M}_2$ type but a linear combination of the form $M = \frac{1}{1+\lambda^2}(M_1 + \lambda M_2) \approx M_1 + \lambda M_2$. Assuming that the Green's functions of the Weyl semimetal with the type-1 and type-2 BCs are g_1 and g_2, respectively, the Green's function g for the mixed BC can be perturbatively obtained for small λ as follows:

$$g = \frac{g_1}{1 + \lambda g_1 M_2} \approx g_1 - \lambda g_1 M_2 g_1, \tag{35}$$

where higher powers of λ are ignored and, due to $\delta(z)$ in Eq. (1), it is understood that the self-energy corrections arising from mixing of the $\check{M}_2$-type boundary condition of strength λ are nonzero only at the interface. The above equation when combined with Eq. (27) gives

$$\det\, g_1 \to \det\, g_1[1 - \lambda\, \mathrm{tr}\, \check{M}_2 g_1]. \tag{36}$$

The poles of which are characterized by $\det g_1$ as long as perturbative thinking is valid to determine the pole of the above renormalized Green's function. Therefore, as long as λ remains within the reach of perturbation theory, the above self-energy arising from chirality flip ($\check{M}_2$) at the interface will only produce a renormalization of spectral features of g_1. So the picture will be as follows: At $\lambda = 0$ (i.e., pure $\check{M}_1$-type BC), we have a robust Bogoliubov Fermi contour. At $\lambda = \infty$ (i.e., pure $\check{M}_2$-type BC), we have the superconducting phase with point nodes in the spectrum of Bogoliubov quasiparticles of the proximitized surface. Therefore, it is likely that a phase transition at a finite λ separates the physics of $\check{M}_1$ from $\check{M}_2$ BCs.

IV. PAIRING SYMMETRY AND MAJORANA FERMI CONTOUR

So far, we have shown that $\check{M}_1$-type BC gives a topologically protected BFC. Now, we are going to discuss its consequences. The Cooper pairs can be either even or odd with respect to its behavior under the exchange of chirality index. In the following, we separately discuss these two cases.

A. Even chirality pairing

It is useful to form combinations of the pairing amplitudes which are even or odd under the exchange of orbital (chirality) index [20]. Each of these Δ's is a 2×2 matrix in spin space and can be written as a sum of singlet and triplet components

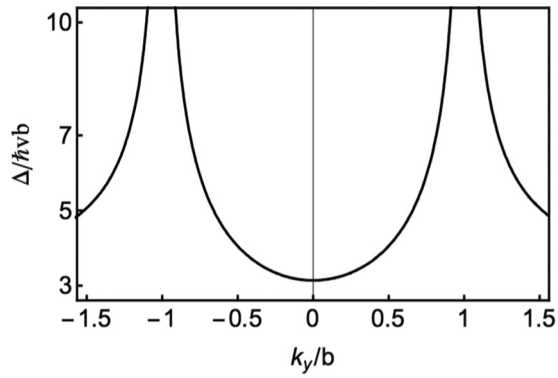

FIG. 3. The k_y dependence of Eq. (40) for $k_x = 0$.

as

$$\hat{\Delta} = i\sigma_y(d_0 + \vec{d}\cdot\vec{\sigma}). \tag{37}$$

The even interorbital part of the anomalous Green's function which is even under the exchange of band index is given by

$$\hat{F}_+ = h\begin{bmatrix} -ik_x + k_y & -b \\ -b & ik_x + k_y \end{bmatrix}, \tag{38}$$

$$h = \frac{4\,\Delta_s k_y s^2[\mathcal{F} - 4b\epsilon s^2(\epsilon - k_y)]}{(\mathcal{F} + 4\epsilon b k_y s^2)^2 - 16\epsilon^2 s^4 k^2}, \tag{39}$$

which gives $d_0 = 0$ and $\vec{d} = (ik_x, -ik_y, -b)h$. The spin-singlet pairing is absent, and therefore, the spin angular momentum of the Cooper pairs is even with respect to the exchange of the spin attribute of the electrons forming the Cooper pair. Since the chirality (band index) is already assumed to be even, the orbital part will be necessarily odd. It is evident from the $\vec{d}$ vector that, in this channel, a substantial $p + ip$ pairing exists. However, it has been multiplied by a factor of h which needs to be integrated over ϵ to give the induced pairing. In the weak tunneling regime where s is small, working to order s^2 which amounts to ignoring s^4 in comparison to s^2 in the numerator, and ignoring s altogether in the denominator, allows us to analytically calculate this function that gives the following strength for the pairing which after restoration of $\hbar$ and v_F will become

$$\Delta \sim \frac{\pi\,\Delta_s s^2 \hbar v_F \sqrt{k_x^2 + k_y^2 + b^2}}{\sqrt{|(\hbar v_F k_y)^2 - \Delta_s^2|}}. \tag{40}$$

This function has been plotted in Fig. 3. On the Fermi arc $k_y = 0$, the induced pairing in its middle $k_x = 0$ is simply $\pi\hbar v_F b s^2$ which conforms to golden rule intuition. Even on the BFC, according to Eq. (30), the minor axis is controlled by s^2, and hence, even on the BFC, k_y remains small. As can be seen in Fig. 3, the k_y dependence near $k_y \approx 0$ is very weak, and therefore, this factor will not introduce higher angular momenta, and the orbital (angular momentum) part will entirely be given by the $p + ip$ form.

B. Odd-chirality pairing

The odd amplitude interorbital pairing is odd under the exchange of the orbital index which is given by

$$\hat{\Delta}_- = \frac{4\,\Delta k_y s^2[\{-4b\epsilon s^2(\epsilon - k_y)]}{(\mathcal{F} + 4\epsilon b k y s^2)^2 - 16\epsilon^2 s^4 k^2}\begin{bmatrix} -ib & -k_x + ik_y \\ -k_x - ik_y & ib \end{bmatrix},$$

with $d_0 = ik_y h$ and $\vec{d} = (-ib, 0, k_x)h$. The integration over energy in the weak tunneling regime gives the same formula (40). Although the singlet pairing amplitude d_0 is zero on the Fermi arc ($k_y = 0$), nevertheless, on the BFC, it acquires a nonzero value. From Eq. (30), this value is proportional to the minor axis $\tilde{b} \propto s^2$. Therefore, the singlet component of pairing on BFC will be controlled by tunneling strength. On the contrary, the triplet component $\vec{d}$ of the induced pairing depends on b and k_x. The z component of this pairing changes from $+b$ to $-b$ by spanning the BFC, whereas its x component remains constant $-ib$. So the BFC is endowed with a nontrivial spin texture for the Cooper pairs.

C. Majorana nature of BFC

The elliptic BFC in our problem is distinct from the underlying Fermi arc. Outside the BFC, the Bogoliubov quasiparticles are more electronlike, whereas, inside the elliptic BFC, the excitations are more holelike. Right on the BFC, the excitations will be equally electronlike and holelike so that the average charge of the excitations is zero. Therefore, the BFC is actually a Majorana Fermi contour. The fact that it is protected by a Z_2 topological index already manifests as the simple fact that changing the tunneling strength s does not destroy the elliptic BFC. It can only modify the aspect ratio and maintains the elliptic shape of the BFC. Now, the question will be as follows: What is the experimental signature of such a Majorana Fermi contour? In a transport setting, the portion of the current which passes through the BFC surface states will appear as a zero-bias feature. At zero temperature, the strength of such a zero-bias peak which is determined by the number of channels is proportional to the perimeter of the Majorana Fermi contour,

$$\frac{dI}{dV} \propto 4bE\left(\frac{1}{\sqrt{1 + 4s^4}}\right), \tag{41}$$

where E is the elliptic function of the second kind and we have restored the length $2b$ of the Fermi arc which determines the major axis of the ellipse. For low temperatures, the peak will acquire thermal broadening but still remains proportional to the above value. According to Ref. [42], the effective length of the Fermi arc can be controlled by coupling to radiation. To this extent, the linear dependence of the above formula to the length $2b$ of the Fermi arc can be checked in transport measurements of illuminated samples.

The BFC will also have clear thermodynamic signature in the specific heat. Since the two-dimensional BFC supports linearly dispersing excitations around it (except for two nodal points which are of measure zero), the resulting density of states will be linear in energy. Therefore, the contribution of these excitations to the specific heat will be $\sim T^2$. This situation is similar to graphene [43]. This can be pleasantly separated from other degrees of freedom that contribute to

absorption of heat. First of all, the bulk degrees of freedom of the superconductor has no subgap excitations. Second, the bulk degrees of freedom of the WSM disperse linearly but in *three* space dimensions. By power counting, they will contribute a T^3 term. Therefore, the T^2 term due to excitations around the BFC will take over at low temperatures and can be separated from the bulk of the WSM and SC.

V. SUMMARY AND DISCUSSION

We have discussed the proximity induced superconductivity in Fermi arc states. By the chirality blockade, the bulk states play no role in the induced superconductivity in the WSM and the resulting transport is dominated by induced superconductivity in surface Fermi arc states. Computing to infinite order in tunneling perturbation theory, we find that the original Fermi arc is completely washed out by coherent all-order tunneling of Cooper pairs from the superconductor into the WSM. However, as a result of this all-order tunneling, a new Bogoliubov Fermi contour is established which is protected by a Z_2 topological index. Such a BFC is actually a Majorana Fermi contour. This Majorana Fermi contour shows up as a zero-bias conductance peak, the strength of which is proportional to the perimeter of the elliptic BFC. This implies linear dependence on the length $2b$ of the Fermi arcs. This Fermi contour is protected from small perturbations. Moreover, in simple specific-heat measurements, the BFC at subgap temperature scales shows up as a distinct T^2 contribution to the heat absorption. This can be separated from the T^3 contribution from bulk states of the WSM. The bulk of the superconductor itself being gapped is out of game in subgap temperature scales. By slightly moving away from the Fermi level, the weight of either hole or electron in the Bogoliubov wave function starts to increase. This might be used for the detection of Bogoliubov bands within ARPES or inverse ARPES measurements. By approaching the Fermi level, the portion of the ARPES signal related to the projection of Bogoliubov states onto hole states will decrease in a characteristic BCS fashion.

For the second type of BC that flips chirality at the boundary instead of BFC, we find pairs of Bogoliubov-Weyl nodes that disperse in the Brillouin zone upon changing the tunneling strength s. The specific-heat signature of Bogoliubov-Weyl nodes is similar to BFC and goes like T^2. The zero-bias conductance peak for first-type BC is expected to be stronger than those of Bogoliubov-Weyl nodes. For the mixed boundary conditions, our perturbative analysis indicates that there can be a phase transition that separates the two types of boundary conditions.

An interesting question that can be put forward is the following: The BFC is a *noninteracting* Fermi contour. What happens when strong interactions are included on top of such a Majorana FC, and what are the possible gap-opening mechanisms? In the case of $p+ip$ pairing, a possible strong-coupling analogous state can be a $\nu = \frac{5}{2}$ quantum Hall state which is expected to develop a pair density wave gap [44].

ACKNOWLEDGMENTS

S.A.J. was supported by Grant No. G960214 from the research deputy of Sharif University of Technology and Iran Science Elites Federation (ISEF). Z.F. was supported by a postdoctoral fellowship from ISEF. We are grateful to M. Kargarin for helpful discussions.

APPENDIX: MATRIX ELEMENTS FOR THE FERMI ARC ALONG THE k_x AXIS

Without loss of generality, one can rotate the coordinates along the k_z axis in such a way that the Fermi arc will lie along the k_x axis. This coordinate system corresponds to setting $\Lambda \to \frac{\pi}{2}$ and $\xi \to \frac{3\pi}{2}$ [20]. So, for electrons, we have

$$k_x^\chi = k_x - \chi b, \quad k_y^\chi = k_y, \quad q_\chi = -\chi k_x + b, \quad \varepsilon = k_y, \tag{A1}$$

and for holes,

$$k_x^\chi = k_x + \chi b, \quad k_y^\chi = k_y, \quad q_\chi = \chi k_x + b, \quad \varepsilon = -k_y. \tag{A2}$$

After these simplifications, for the $\check{M}_1$-type BC, we have

$$\begin{aligned}
\left[G^{\bar\sigma\sigma}_{\chi\chi}\right]_e &= \left(\frac{-i\sigma}{4\pi^2}\right)\frac{k_x - \chi b + i\sigma k_y}{\varepsilon - k_y} e^{(\chi k_x - b)(z+z')}\Theta(\bar\chi k_x), \quad \left[G^{\sigma\sigma}_{\chi\chi}\right]_e = \left(\frac{-\chi}{4\pi^2}\right)\frac{k_x - \chi b + i\sigma k_y}{\varepsilon - k_y} e^{(\chi k_x - b)(z+z')}\Theta(\bar\chi k_x),\\
\left[G^{\bar\sigma\sigma}_{\chi\chi}\right]_h &= \left(\frac{i\sigma}{4\pi^2}\right)\frac{k_x + \chi b - i\sigma k_y}{\varepsilon + k_y} e^{(-\chi k_x - b)(z+z')}\Theta(\chi k_x), \quad \left[G^{\sigma\sigma}_{\chi\chi}\right]_h = \left(\frac{-\chi}{4\pi^2}\right)\frac{k_x + \chi b - i\sigma k_y}{\varepsilon + k_y} e^{(-\chi k_x - b)(z+z')}\Theta(\chi k_x).
\end{aligned} \tag{A3}$$

So, the elements of the Green's function matrices for electrons and holes are obtained as follows:

$$\begin{aligned}
[G^{\uparrow\uparrow(\downarrow\downarrow)}_{++}]_e &= \left(\frac{-1}{4\pi^2}\right)\frac{k_x - b \pm ik_y}{\varepsilon - k_y} e^{(k_x - b)(z+z')}\Theta_R, \quad [G^{\uparrow\uparrow(\downarrow\downarrow)}_{--}]_e = \left(\frac{1}{4\pi^2}\right)\frac{k_x + b \pm ik_y}{\varepsilon - k_y} e^{(-k_x - b)(z+z')}\Theta_L,\\
[G^{\uparrow\downarrow(\downarrow\uparrow)}_{++}]_e &= \left(\frac{\pm i}{4\pi^2}\right)\frac{k_x - b \mp ik_y}{\varepsilon - k_y} e^{(k_x - b)(z+z')}\Theta_R, \quad [G^{\uparrow\downarrow(\downarrow\uparrow)}_{--}]_e = \left(\frac{\pm i}{4\pi^2}\right)\frac{k_x + b \mp ik_y}{\varepsilon - k_y} e^{(-k_x - b)(z+z')}\Theta_L,\\
[G^{\uparrow\uparrow(\downarrow\downarrow)}_{++}]_h &= \left(\frac{-1}{4\pi^2}\right)\frac{k_x + b \mp ik_y}{\varepsilon + k_y} e^{(-k_x - b)(z+z')}\Theta_L, \quad [G^{\uparrow\uparrow(\downarrow\downarrow)}_{--}]_h = \left(\frac{1}{4\pi^2}\right)\frac{k_x - b \mp ik_y}{\varepsilon + k_y} e^{(k_x - b)(z+z')}\Theta_R,
\end{aligned}$$

$$[G^{\uparrow\downarrow(\downarrow\uparrow)}_{++}]_h = \left(\frac{\mp i}{4\pi^2}\right)\frac{k_x + b \pm ik_y}{\varepsilon + k_y} e^{(-k_x - b)(z+z')}\Theta_L, \quad [G^{\uparrow\downarrow(\downarrow\uparrow)}_{--}]_h = \left(\frac{\mp i}{4\pi^2}\right)\frac{k_x - b \pm ik_y}{\varepsilon + k_y} e^{(k_x - b)(z+z')}\Theta_R, \tag{A4}$$

and for the $\check{M}_2$-type boundary,

$$\begin{aligned}
\left[G^{\bar{\sigma}\sigma}_{\chi\chi}\right]_e &= -\left(\frac{i\chi\sigma}{8\pi^2 b}\right)\frac{(k_x + i\sigma k_y)^2 - b^2}{\varepsilon - k_y} e^{(\chi k_x - b)(z+z')}\Theta(\chi k_x < 0),\\
\left[G^{\sigma\sigma}_{\chi\chi}\right]_e &= \left(\frac{-1}{8\pi^2 b}\right)\frac{(k_x + i\sigma k_y)^2 - b^2}{\varepsilon - k_y} e^{(\chi k_x - b)(z+z')}\Theta(\chi k_x < 0),\\
\left[G^{\bar{\sigma}\sigma}_{\bar{\chi}\chi}\right]_e &= \left(\frac{1}{16\pi^2 b}\right)\frac{(k_x + i\sigma k_y)^2 - b^2}{\varepsilon - k_y} e^{(\chi k_x - b)(z+z')}\Theta(\chi k_x < 0),\\
\left[G^{\sigma\sigma}_{\bar{\chi}\chi}\right]_e &= -\left(\frac{i\chi\sigma}{16\pi^2 b}\right)\frac{(k_x - \chi b)^2 + k_y^2}{\varepsilon - k_y} e^{(\chi k_x - b)(z+z')}\Theta(\chi k_x < 0),
\end{aligned} \tag{A5}$$

$$\begin{aligned}
\left[G^{\bar{\sigma}\sigma}_{\chi\chi}\right]_h &= \left(\frac{i\chi\sigma}{8\pi^2 b}\right)\frac{(k_x - i\sigma k_y)^2 - b^2}{\varepsilon + k_y} e^{-(\chi k_x + b)(z+z')}\Theta(\chi k_x > 0),\\
\left[G^{\sigma\sigma}_{\chi\chi}\right]_h &= \left(\frac{1}{8\pi^2 b}\right)\frac{(k_x - i\sigma k_y)^2 - b^2}{\varepsilon + k_y} e^{-(\chi k_x + b)(z+z')}\Theta(\chi k_x > 0),\\
\left[G^{\bar{\sigma}\sigma}_{\bar{\chi}\chi}\right]_h &= \left(\frac{1}{16\pi^2 b}\right)\frac{(k_x - i\sigma k_y)^2 - b^2}{\varepsilon + k_y} e^{-(\chi k_x + b)(z+z')}\Theta(\chi k_x > 0),\\
\left[G^{\sigma\sigma}_{\bar{\chi}\chi}\right]_h &= \left(\frac{i\chi\sigma}{16\pi^2 b}\right)\frac{(k_x + \chi b)^2 + k_y^2}{\varepsilon + k_y} e^{-(\chi k_x + b)(z+z')}\Theta(\chi k_x > 0).
\end{aligned} \tag{A6}$$

Expanding the spin components of the matrix, we have

$$[G^{\uparrow\uparrow(\downarrow\downarrow)}_{++}]_e = \left(\frac{-1}{8\pi^2 b}\right)\frac{(k_x \pm i\,k_y)^2 - b^2}{\varepsilon - k_y} e^{(k_x - b)(z+z')}\Theta_R, \quad [G^{\uparrow\uparrow(\downarrow\downarrow)}_{--}]_e = \left(\frac{-1}{8\pi^2 b}\right)\frac{(k_x \pm ik_y)^2 - b^2}{\varepsilon - k_y} e^{-(k_x + b)(z+z')}\Theta_L,$$

$$[G^{\uparrow\downarrow(\downarrow\uparrow)}_{++}]_e = \left(\frac{\pm i}{8\pi^2 b}\right)\frac{(k_x \mp ik_y)^2 - b^2}{\varepsilon - k_y} e^{(k_x - b)(z+z')}\Theta_R, \quad [G^{\uparrow\downarrow(\downarrow\uparrow)}_{--}]_e = \left(\frac{\mp i}{8\pi^2 b}\right)\frac{(k_x \mp ik_y)^2 - b^2}{\varepsilon - k_y} e^{-(k_x + b)(z+z')}\Theta_L, \tag{A7}$$

$$[G^{\uparrow\uparrow(\downarrow\downarrow)}_{+-}]_e = \left(\frac{\pm i}{16\pi^2 b}\right)\frac{(k_x + b)^2 + k_y^2}{\varepsilon - k_y} e^{-(k_x + b)(z+z')}\Theta_L, \quad [G^{\uparrow\uparrow(\downarrow\downarrow)}_{-+}]_e = \left(\frac{\mp i}{16\pi^2 b}\right)\frac{(k_x - b)^2 + k_y^2}{\varepsilon - k_y} e^{(k_x - b)(z+z')}\Theta_R,$$

$$[G^{\uparrow\downarrow(\downarrow\uparrow)}_{+-}]_e = \left(\frac{1}{16\pi^2 b}\right)\frac{(k_x \mp ik_y)^2 - b^2}{\varepsilon - k_y} e^{-(k_x + b)(z+z')}\Theta_L, \quad [G^{\uparrow\downarrow(\downarrow\uparrow)}_{-+}]_e = \left(\frac{1}{16\pi^2 b}\right)\frac{(k_x \mp ik_y)^2 - b^2}{\varepsilon - k_y} e^{(k_x - b)(z+z')}\Theta_R,$$

$$[G^{\uparrow\uparrow(\downarrow\downarrow)}_{++}]_h = \left(\frac{1}{8\pi^2 b}\right)\frac{(k_x \mp ik_y)^2 - b^2}{\varepsilon + k_y} e^{-(k_x + b)(z+z')}\Theta_L, \quad [G^{\uparrow\uparrow(\downarrow\downarrow)}_{--}]_h = \left(\frac{1}{8\pi^2 b}\right)\frac{(k_x \mp ik_y)^2 - b^2}{\varepsilon + k_y} e^{(k_x - b)(z+z')}\Theta_R,$$

$$[G^{\uparrow\downarrow(\downarrow\uparrow)}_{++}]_h = \left(\frac{\mp i}{8\pi^2 b}\right)\frac{(k_x \pm ik_y)^2 - b^2}{\varepsilon + k_y} e^{-(k_x + b)(z+z')}\Theta_L, \quad [G^{\uparrow\downarrow(\downarrow\uparrow)}_{--}]_h = \left(\frac{\pm i}{8\pi^2 b}\right)\frac{(k_x \pm ik_y)^2 - b^2}{\varepsilon + k_y} e^{(k_x - b)(z+z')}\Theta_R,$$

$$[G^{\uparrow\uparrow(\downarrow\downarrow)}_{+-}]_h = \left(\frac{\mp i}{16\pi^2 b}\right)\frac{(k_x - b)^2 + k_y^2}{\varepsilon + k_y} e^{(k_x - b)(z+z')}\Theta_R, \quad [G^{\uparrow\uparrow(\downarrow\downarrow)}_{-+}]_h = \left(\frac{\pm i}{16\pi^2 b}\right)\frac{(k_x + b)^2 + k_y^2}{\varepsilon + k_y} e^{-(k_x + b)(z+z')}\Theta_L,$$

$$[G^{\uparrow\downarrow(\downarrow\uparrow)}_{+-}]_h = \left(\frac{1}{16\pi^2 b}\right)\frac{(k_x \pm ik_y)^2 - b^2}{\varepsilon + k_y} e^{(k_x - b)(z+z')}\Theta_R, \quad [G^{\uparrow\downarrow(\downarrow\uparrow)}_{-+}]_h = \left(\frac{1}{16\pi^2 b}\right)\frac{(k_x \pm ik_y)^2 - b^2}{\varepsilon + k_y} e^{-(k_x + b)(z+z')}\Theta_L. \tag{A8}$$

[1] A. A. Burkov, M. D. Hook, and L. Balents, Phys. Rev. B **84**, 235126 (2011).

[2] S. Murakami, New J. Phys. **9**, 356 (2007).

[3] X. Wan, A. M. Turner, A. Vishwanath, and S. Y. Savrasov, Phys. Rev. B **83**, 205101 (2011).

[4] L. Lu, Z. Wang, D. Ye, L. Ran, L. Fu, J. D. Joannopoulos, and M. Soljačić, Science **349**, 622 (2015).

[5] B. Q. Lv, H. M. Weng, B. B. Fu, X. P. Wang, H. Miao, J. Ma, P. Richard, X. C. Huang, L. X. Zhao, G. F. Chen, Z. Fang, X. Dai, T. Qian, and H. Ding, Phys. Rev. X **5**, 031013 (2015).

[6] A. A. Burkov and L. Balents, Phys. Rev. Lett. **107**, 127205 (2011).

[7] C. Fang, M. J. Gilbert, X. Dai, and B. A. Bernevig, Phys. Rev. Lett. **108**, 266802 (2012).

[8] G. B. Halász and L. Balents, Phys. Rev. B **85**, 035103 (2012).
[9] S. M. Young, S. Zaheer, J. C. Y. Teo, C. L. Kane, E. J. Mele, and A. M. Rappe, Phys. Rev. Lett. **108**, 140405 (2012).
[10] P. Delplace, J. Li, and D. Carpentier, Euro. Phys. Lett. **97**, 67004 (2012).
[11] T. Ojanen, Phys. Rev. B **87**, 245112 (2013).
[12] A. M. Turner and A. Vishwanath, arXiv:1301.0330.
[13] S.-M. Huang, S.-Y. Xu, I. Belopolski, C.-C. Lee, G. Chang, B. Wang, N. Alidoust, G. Bian, M. Neupane, C. Zhang, S. Jia, A. Bansil, H. Lin, and M. Z. Hasan, Nat. Commun. **6**, 7373 (2015).
[14] S. Xu, C. Liu, S. K. Kushwaha, R. Sankar, J. W. Krizan, I. Belopolski, M. Neupane, G. Bian, N. Alidoust, T. Chang, H. Jeng, C. Huang, W. Tsai, H. Lin, F. Chou, P. P. Shibayev, R. J. Cava, and M. Z. Hasan, Science **347**, 294 (2015).
[15] S.-Y. Xu, I. Belopolski, N. Alidoust, M. Neupane, G. Bian, C. Zhang, R. Sankar, G. Chang, Z. Yuan, C.-C. Lee, S.-M. Huang, H. Zheng, J. Ma, D. S. Sanchez, B. Wang, A. Bansil, F. Chou, P. P. Shibayev, H. Lin, S. Jia, and M. Z. Hasan, Science **349**, 613 (2015).
[16] In WSMs that preserve the time-reversal symmetry, the bulk states contribute to the Josephson current, and there is no chirality blockade. See, e.g., S.-B. Zhang, J. Erdmenger, and B. Trauzettel, Phys. Rev. Lett. **121**, 226604 (2018).
[17] N. Bovenzi, M. Breitkreiz, P. Baireuther, T. E. O'Brien, J. Tworzydło, I. Adagideli, and C. W. J. Beenakker, Phys. Rev. B **96**, 035437 (2017).
[18] H. Wei, S.-P. Chao, and V. Aji, Phys. Rev. B **89**, 014506 (2014).
[19] Y. Kim, M. J. Park, and M. J. Gilbert, Phys. Rev. B **93**, 214511 (2016).
[20] Z. Faraei and S. A. Jafari, Phys. Rev. B **96**, 134516 (2017).
[21] M. Salehi and S. A. Jafari, Sci. Rep. **7**, 8221 (2017).
[22] W. Chen, L. Jiang, R. Shen, L. Sheng, B. G. Wang, and D. Y. Xing, Europhys. Lett. **103**, 27006 (2013).
[23] U. Khanna, D. K. Mukherjee, A. Kundu, and S. Rao, Phys. Rev. B **93**, 121409(R) (2016).
[24] K. A. Madsen, E. J. Bergholtz, and P. W. Brouwer, Phys. Rev. B **95**, 064511 (2017).
[25] S. Uchida, T. Habe, and Y. Asano, J. Phys. Soc. Jpn. **83**, 064711 (2014).
[26] T. Zhou, Y. Gao, and Z. D. Wang, Phys. Rev. B **98**, 024515 (2018).
[27] B. Huang, Eur. Phys. J. B **90**, 131 (2017).
[28] B. Lu, K. Yada, M. Sato, and Y. Tanaka, Phys. Rev. Lett. **114**, 096804 (2015).
[29] Y. Li and F. D. M. Haldane, Phys. Rev. Lett. **120**, 067003 (2018).
[30] M. D. Schwartz, *Quantum Field Theory and the Standard Model* (Cambridge University Press, Cambridge, UK, 2014).
[31] S. Rao, arXiv:1603.02821.
[32] Z. Faraei, T. Farajollahpour, and S. A. Jafari, Phys. Rev. B **98**, 195402 (2018).
[33] E. McCann and V. I. Falko, J. Phys.: Condens. Matter **16**, 2371 (2004).
[34] A. R. Akhmerov and C. W. J. Beenakker, Phys. Rev. B **77**, 085423 (2008).
[35] U. Khanna, A. Kundu, S. Pradhan, and S. Rao, Phys. Rev. B **90**, 195430 (2014).
[36] D. F. Agterberg, P. M. R. Brydon, and C. Timm, Phys. Rev. Lett. **118**, 127001 (2017).
[37] P. M. R. Brydon, D. F. Agterberg, H. Menke, and C. Timm, Phys. Rev. B **98**, 224509 (2018).
[38] A. P. Schnyder, S. Ryu, A. Furusaki, and A. W. W. Ludwig, Phys. Rev. B **78**, 195125 (2008).
[39] C.-K. Chiu, J. C. Y. Teo, A. P. Schnyder, and S. Ryu, Rev. Mod. Phys. **88**, 035005 (2016).
[40] A. Altland and M. R. Zirnbauer, Phys. Rev. B **55**, 1142 (1997).
[41] G. E. Volovik, *The Universe in a Helium Droplet*, International Series of Monographs on Physics, 1st ed. (Clarendon, Oxford, 2003), Vol. 117.
[42] U. Khanna, S. Rao, and A. Kundu, Phys. Rev. B **95**, 201115(R) (2017).
[43] E. Pop, V. Varshney, and A. K. Roy, MRS Bull. **37**, 1273 (2012).
[44] M. McGinley and N. R. Cooper, Phys. Rev. B **99**, 075148 (2019).